
GARG-AML AGAINST SMURFING: A SCALABLE AND INTERPRETABLE GRAPH-BASED FRAMEWORK FOR ANTI-MONEY LAUNDERING

A PREPRINT

Bruno Deprez*
KU Leuven
University of Antwerp - imec

Bart Baesens
KU Leuven
University of Southampton

Tim Verdonck
University of Antwerp - imec
KU Leuven

Wouter Verbeke
KU Leuven

ABSTRACT

Money laundering poses a significant challenge as it is estimated to account for 2%–5% of the global GDP. This has compelled regulators to impose stringent controls on financial institutions. One prominent laundering method for evading these controls, called smurfing, involves breaking up large transactions into smaller amounts. Given the complexity of smurfing schemes, which involve multiple transactions distributed among diverse parties, network analytics has become an important anti-money laundering tool. However, recent advances have focused predominantly on black-box network embedding methods, which has hindered their adoption in businesses. In this paper, we introduce GARG-AML, a novel graph-based method that quantifies smurfing risk through a single interpretable metric derived from the structure of the second-order transaction network of each individual node in the network. Unlike traditional methods, GARG-AML strikes an effective balance among computational efficiency, detection power and transparency, which enables its integration into existing AML workflows. To enhance its capabilities, we combine the GARG-AML score calculation with different tree-based methods and also incorporate the scores of the node’s neighbours. An experimental evaluation on large-scale synthetic and open-source networks demonstrate that the GARG-AML outperforms the current state-of-the-art smurfing detection methods. By leveraging only the adjacency matrix of the second-order neighbourhood and basic network features, this work highlights the potential of fundamental network properties towards advancing fraud detection.

Keywords Fraud Analytics · Anti-Money Laundering · Network Analytics · Smurfing · Microstructuring

1 Introduction

Money laundering disguises illegally-obtained funds, often from criminal activities, to make them appear legitimate. Once cleaned, the money can be used to finance further crimes. Estimates put the amount of laundered money at 2% to 5% of global GDP, which amounts to USD 2 trillion annually [42]. Since laundering money involves interactions with and through the normal financial system, regulators have imposed stringent anti-money laundering (AML) rules on financial institutions [16, 26].

Money laundering involves three main steps [42, 26]. **Placement** refers to the introduction of funds into the financial system. During **layering**, money is moved around to obscure its illegal origins. Finally, **integration** is the incorporation of laundered money into broader circulation. Because of the involvement of different steps and actors, network analytics has become an important tool for AML [11].

A popular money laundering method is *smurfing* [30, 46, 39, 51]. Large transactions between two accounts are often flagged according to business rules [6, 37, 34] in accordance with regulation [46]. Therefore, transactions are split into smaller amounts and transferred using multiple money mules—also called smurfs—making detection of illicit money flows harder since (1) the origin of the funds is obscured and (2) smaller transactions seem less suspicious.

*Corresponding author: bruno.deprez@kuleuven.be

Two types of patterns are typical for smurfing [39]: (1) scatter-gather and (2) gather-scatter [3]. Both patterns are visualised in Figure 1. With scatter-gather, money is sent to its destination account via money mules. Gather-scatter, on the other hand, consists of collecting money from multiple accounts into one (or a few) account(s) and sending it to many destination accounts. Gather-scatter is a popular money laundering method for cryptocurrencies [48].

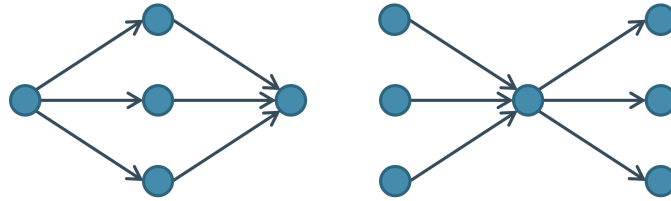


Figure 1: The two smurfing patterns described in the literature [39, 3]; as scatter-gather (left) and gather-scatter (right).

To fight money laundering, AML practices use customer and transaction data to estimate each client’s money laundering propensity. When suspicion is raised, investigators build a suspicious activity report (SAR) to file with the regulator [16, 26]. Given the vast volume of monitored transactions and the involvement of different business departments in filing a SAR, two aspects are key to ensuring the effective business adoption of a method:

- The method must process large volumes of transactions in a memory and time efficient manner;
- The predictions must be interpretable for smooth integration in SAR filing.

Despite these business requirements, the current AML literature often focuses on deep graph neural networks (GNNs) [11]. GNNs are, however, not interpretable, prohibiting the adoption of these novel network analytics methods in practice. Consequently, many institutions still rely on business rules and manual feature engineering based on expert knowledge, which are expensive to maintain and easy to evade.

Given the specific nature of smurfing and the operational requirements faced by financial institutions, we introduce **Graph-Aided Risk Grading for Anti-Money Laundering (GARG-AML)**, a novel method that grades clients on the basis of their second-order neighbourhood in the transaction network. GARG-AML operates by analysing the resulting adjacency matrix and computing scores based on the contrast between high-density and low-density regions to quantify the network’s resemblance to smurfing. We introduce two versions of GARG-AMM, one based on directed and one on undirected transaction networks.

Moreover, we present an extension to the base GARG-AML score, increasing smurf detection power by combining GARG-AML with classic network centrality measures and tree-based learners. This shows the versatility and power of our method, without compromising on the business needs of speed and simplicity.

The performance of GARG-AML and its extensions is evaluated against state-of-the-art smurfing detection methods using both synthetic and two open-source network datasets. These datasets, which include millions of clients and transactions, closely resemble real-world financial networks. As a result, our experiments assess both detection accuracy and computational efficiency.

The main contributions of this work are as follows:

- We introduce a novel smurfing detection method that is scalable to large transaction networks, interpretable and easily integrated into existing machine learning models;
- We evaluate our method on multiple datasets which are uniquely suited for assessing the effectiveness of our approach;
- We compare the current state-of-the-art smurfing detection methods, and we perform the first analysis of the scalability of these methods to very large transaction datasets.

The remainder of this work is organised as follows. Related work on anti-money laundering and smurfing is discussed in Section 2. The methodology behind the GARG-AML score calculation is described in Section 3. Section 4 outlines the experimental evaluation, and the results are presented in Section 5. We discuss the main limitations in Section 6, in terms of both the data in general and GARG-AML in particular. Section 7 concludes this work.

Complete implementations of the methods and experiments are provided on GitHub² to promote further adoption of and experimentation on the GARG-AML scores by peer researchers and practitioners.

²<https://github.com/B-Deprez/GARG-AML>

2 Related Work

Anti-money laundering (AML), like other areas of financial fraud detection, traditionally relied on IF-THEN business rules—combinations of expert knowledge and regulatory requirements [6, 25, 36, 46, 7, 11]. These rules typically monitor individual transactions or aggregated amounts over time [16]. While offering transparency in decision-making [52], they are costly to maintain [43] and can be easily circumvented once exposed. As a result, machine learning has emerged as a preferred approach, offering scalability and the ability to detect complex laundering patterns [8].

To capture interactions among people, network analytics for AML has been studied extensively in recent years [11]. Research has often relied on manual network feature engineering for profile definition. Dreżewski et al. [12] used different centrality measures, which resulted in nine roles in a criminal network. Fronzetti Colladon and Remondi [20] used similar metrics across industries and analysed the correlation with the target label to demonstrate the added value of network analytics for AML. Wu et al. [47] define temporal motives specifically tailored to money laundering and mixing detection in the Bitcoin network.

In addition to manual feature engineering, graph neural networks (GNNs) have also been studied extensively [29, 2, 45, 11]. These methods capture the complex geometry of suspicious money laundering activities in financial networks by learning network topology while also incorporating node features. A drawback is that GNNs are not interpretable [22], which limits their use by investigators when filing their reports.

Smurfing has long been a popular laundering method [46, 37]. Welling [46] suggested that it has been applied since 1970, when the Bank Secrecy Act was passed in the USA, which required reporting of transactions above \$10,000. To this day, similar rule-based systems are in place that require immediate investigation of transactions that surpass a given amount [37, 34, 6].

Research has already been conducted on smurfing detection. Zhdanova et al. [51] introduced PSA@R for detecting smurfing in mobile money networks. It uses different underlying workflow models. Transaction streams that differ from the process model are flagged as anomalous. Additional criteria are applied to find money mules on the basis of the difference in the amounts of money coming into and going out of an account.

FlowScope [27] tries to find anomalous sub-graphs on the basis of money flow. The authors constructed a k -partite network with two sets of nodes: nodes with net inflow to or net outflow from the bank and the remaining nodes, which correspond to the middle men. Li et al. [27] defined their anomaly score on the basis of the difference between the inflow and outflow of money at these middle men, and they claimed that smurfs transfer almost all the money they receive.

A similar idea was put forward with AutoAudit [24]. The full adjacency matrix of the network is reordered, and depending on the density of the different blocks, a group of transactions is flagged as smurfing.

Starnini et al. [39] presented a method that merges two transaction datasets and retains only those connections where both transactions occur within a specific time window. Prior to this merger, a substantial amount of data, i.e., nodes deemed trustworthy by the bank together with a majority of transactions, is discarded. After merging, the method retains certain motifs and applies an additional post-processing step, which then triggers manual investigations by AML experts.

SMoTeF [38] is a three-step approach. The first is smurfing pattern extraction, using existing methods. The novelty comes from the second and third steps, where the patterns are checked against temporal constraints and maximal money flow, respectively. Many transactions are again pruned before making final predictions.

Closely related to smurfing is mixing, which is a money laundering method that is used for cryptocurrencies [28]. Coins are transferred to the same entity and are redistributed afterward [48]. This obfuscates the history of ownership, which results in an inability to know the money’s real origin. Mixing can be viewed as the second smurfing pattern in Figure 1, i.e., gather-scatter.

An anomaly score for mixing detection was introduced by Prado-Romero et al. [35]. The authors claimed that mixing services act as bridges between communities in a transaction network by linking otherwise unrelated users. After community detection, the anomaly score expresses the difference in a node’s intercommunity links compared with those of the other nodes in the same community.

Wu et al. [47] constructed two networks for network feature extraction. The first links accounts using their transactions, whereas the second network represents both accounts and transactions as nodes to leverage transaction information. The extracted network features are based on predefined temporal motifs, which are added to the account and transaction features to detect smurfing in a positive and unlabelled (PU)-learning setting.

Table 1: Summary of key aspects of the methodology in the literature.

Paper	Pattern	Client Scoring	Parallel Calculation	All Nodes	Code	Scalable
Zhdanova et al. [51]	Scatter-gather	✓	✓	✓		
Li et al. [27]	Scatter-gather			✓	✓	✓
Lee et al. [24]	Scatter-gather	✓			✓	
Starnini et al. [39]	Scatter-gather & gather-scatter		✓			✓
Shadrooh and Nørnvåg [38]	Scatter-gather	✓				✓
Prado-Romero et al. [35]	Gather-scatter	✓	✓	✓		
Wu et al. [47]	Gather-scatter					✓
This work	Scatter-gather & gather-scatter	✓	✓	✓	✓	✓

Table 2: Summary of key aspects of the experimental set-ups in the literature

Paper	Dataset	Size Dataset (nodes)	Metrics
Zhdanova et al. [51]	Simulated	10,000	Precision, recall
Li et al. [27]	Proprietary & Czech Financial	6,130,000 & 11,374	F1, Time
Lee et al. [24]	Czech Financial & Enron	11,374 & 16,771	Accuracy
Starnini et al. [39]	Proprietary	18,000,000 (reduced to 21,000)	Time
Shadrooh and Nørnvåg [38]	Czech Financial & Enron & Darpa	11,374 & 16,771 & 371,000	Time, Precision, Recall, F1
Prado-Romero et al. [35]	Bitcoin	942,204	Recall
Wu et al. [47]	WalletExplorer	±2, 500, 000	TPR, FPR, geometric mean
This work	Simulated & IBM AML	100 & 10,000 & 100,000 & 515,080 & 2,054,390	Time, AUC-ROC, AUC-PR, Rank

The above literature is summarised and juxtaposed against our proposed method according to the methodology in Table 1 and according to the experimental set-up in Table 2. As expected, most methods for anti-money laundering on fiat currency consider only scatter-gather patterns, while research on crypto-currency is mostly concerned with gather-scatter.

The evaluation in most papers is done on relatively small datasets, making it harder to judge whether they scale well to the massive transaction networks faced by financial institutions. The dataset that was used in most of the above papers is the Czech dataset [1], which is a rather small network that contains approximately 11,000 nodes and approximately 273,000 edges. This dataset is unlabelled, so the authors of each paper inject synthetic pattern. Additionally, in most papers, evaluation and comparison is limited to threshold-dependent metrics like precision, recall and F1.

In this paper, we propose a new method that scores all clients individually, where score can be calculated in parallel. These score can also be used both for scatter-gather as well as for gather-scatter patterns. The experiments are done on very large, realistic data, where we use threshold-independent metrics that allow us to have a comprehensive comparison among the methods under consideration.

3 GARG-AML

3.1 Preliminaries and Notation

A network $G(V, E)$ is defined by a set of nodes, $V = \{v_1, \dots, v_k\}$, and a set of edges, $E \subset V \times V$. The edges can be represented using the adjacency matrix, A , where the elements are defined as

$$A_{ij} = \begin{cases} 1 & \text{if } (v_i, v_j) \in E \\ 0 & \text{elsewhere} \end{cases}$$

Suppose $\mathcal{N}_k(v)$ represents the set of nodes that are at distance exactly k from node v . For GARG-AML, we consider the neighbours of each node v at distances one and two, i.e., $\mathcal{N}_1(v)$ and $\mathcal{N}_2(v)$, respectively. Suppose that $|\mathcal{N}_1(v)| = n$ and $|\mathcal{N}_2(v)| = m - 1$; then, the adjacency matrix of the second-order neighbourhood of v is of size $(m + n) \times (m + n)$.

3.2 Undirected

We introduce GARG-AML using the smurfing pattern defined by Starnini et al. [39] and illustrated in Figure 2. The full GARG-AML method is given in Algorithm 1. Given node A , the corresponding adjacency matrix - defined in Equation (1) - is constructed by arranging the nodes in a specific order: node A is placed first, followed by the second-order neighbour E , and then its first-order neighbours B, C and D . This ordering results in an adjacency matrix that is divided into four distinct blocks. The diagonal blocks contain only zeros, whereas the off-diagonal blocks contain ones.

In this example, we will consider only the gather-scatter pattern, as this is most widely recognised as smurfing. The GARG-AML calculations and node order stay the same in the gather-scatter case.

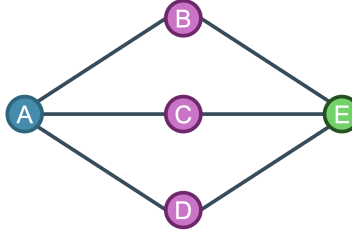


Figure 2: Example of a smurfing pattern. A is the node that will receive the score. The first-order neighbours (B, C, D) are shown in purple, and the second-order neighbour (E) is shown in green.

$$\begin{array}{l}
 A \\
 E \\
 B \\
 C \\
 D
 \end{array}
 \begin{pmatrix}
 0 & 0 & 1 & 1 & 1 \\
 0 & 0 & 1 & 1 & 1 \\
 1 & 1 & 0 & 0 & 0 \\
 1 & 1 & 0 & 0 & 0 \\
 1 & 1 & 0 & 0 & 0
 \end{pmatrix}
 \quad (1)$$

In general, the first row of the adjacency matrix, which corresponds to entries $(A_{1,j})$, represents the connections of node v under consideration. The next $m - 1$ rows, $(A_{i,j})$ for $2 \leq i \leq m$, represent the connections of nodes that are located at a distance of two from v . The final n rows, entries $(A_{i,j})$ for $m + 1 \leq i \leq m + n$, represent the connections of nodes at a distance of one from v .

By enforcing this node ordering—the target node, second-order neighbours, and first-order neighbours—for the adjacency matrix, we ensure that when a pure smurfing pattern is present, the diagonal blocks remain sparse (low density), and the off-diagonal blocks have a high density. The exact order of nodes within each group is not important. For example, any permutation within the first-order neighbours, such as C, B, D , is equally valid.

We consider three primary blocks of the adjacency matrix for score calculation: the upper-left, upper-right, and lower-right blocks. These are defined as follows:

$$\text{block}_1 = (A_{i,j})_{1 \leq i, j \leq m} \quad (2)$$

$$\text{block}_2 = (A_{i,j})_{1 \leq i \leq m, m+1 \leq j \leq m+n} \quad (3)$$

$$\text{block}_3 = (A_{i,j})_{m+1 \leq i, j \leq m+n} \quad (4)$$

GARG-AML measures the similarity between an observed pattern and the pure smurfing template by analysing the expected density and actual density (or sparsity) of each block. This results in a single quantitative score expressing similarity to the pure smurfing pattern.

In computing these densities, several structural properties of the adjacency matrix are taken into account. First, self-loops are excluded; thus, diagonal elements are always zero and are omitted from the sparsity/density calculations. Furthermore, in block_1 (upper-left block), the first row and column can never contain ones, as a ‘1’ would indicate a direct connection between a node and its second-order neighbours—a contradiction. This block serves as a check that the nodes at distance two do not directly make transactions to each other, in case multiple nodes at a distance of two are present. Similarly, for block_2 (upper-right block), all the elements in the first row must be ones since these represent connections between the central node and its first-order neighbours.

These structural constraints affect both the numerator and denominator in the density calculations. Accordingly, when computing block-wise densities, we consider only the valid entries, and the block sizes (denominators) are normalised to reflect this. On the basis of the observations above, smurfing is likely to be present when the density of block_2 (upper-right block) is high, while block_1 (upper-left block) and block_3 (lower-right) exhibit densities close to zero. This

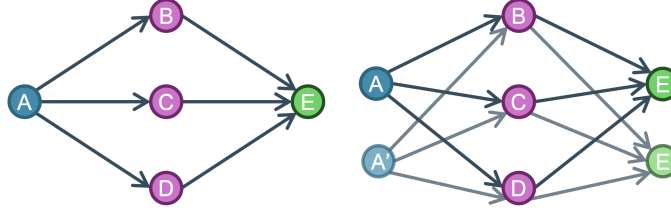


Figure 3: The directed version of the smurfing pattern example, extended with an additional sending node (A') and receiving node (E'). Nodes at level 0 are put in blue, at level 1 in purple and at level 2 in green.

is reflected in the final score as follows:

$$\text{score}_1 = \frac{\text{sum}(\text{block}_1)}{m^2 - 3m + 2} \quad (5)$$

$$\text{score}_2 = \frac{\text{sum}(\text{block}_2) - m}{mn - n} \quad (6)$$

$$\text{score}_3 = \frac{\text{sum}(\text{block}_3)}{n^2 - n} \quad (7)$$

$$\text{score}_{\text{total}} = \text{score}_2 - \frac{l_1 \cdot \text{score}_1 + l_3 \cdot \text{score}_3}{l_1 + l_3} \quad (8)$$

The inclusion of l_i increases the flexibility of the score calculation. If $l_i = 1$, the score is the average of score_1 and score_3 . In our experiments, however, we take the weighted average by setting:

$$\begin{aligned} l_1 &= m^2 - 3m + 2 \\ l_3 &= n^2 - n. \end{aligned}$$

When there is only one destination account, there is only one node at distance two (as in Figure 2), which results in l_1 being 0. We take the weighted average because we need to compare only score_2 to score_3 .

The final score in Equation (8) ranges from -1 to 1 . When the second-order neighbourhood resembles a smurfing pattern, the final score is close to 1 .

3.3 Directed

A defining trait of smurfing is the unidirectional flow of funds—money moves from one account to others with minimal or no return flow [39, 24, 27, 38], forming what we call *pure smurfing* patterns (see Figure 3). To capture this behaviour, we extend GARG-AML to directed networks.

In the directed network of Figure 3, unlike the undirected case (Figure 2), node A only sends funds to smurfs, while node E only receives them. This asymmetry leads to a non-symmetric adjacency matrix, requiring nine matrix blocks instead of three (see Equation (10)). To ensure consistency in block-wise density calculations—especially with multiple senders or receivers—we distinguish senders (level 0) from receivers (level 2), as shown in Figure 3.

Accordingly, we define two types of second-order neighbourhoods in network $G(V, E)$. The *strong* second-order neighbourhood, denoted $\mathcal{N}_2^s(v)$, considers nodes reachable from v via a directed path of length two. The *weak* second-order neighbourhood, $\mathcal{N}_2^w(v)$, uses the undirected network. In both, only nodes at exact distance two are included.

A node w is assigned to level 0 if

$$w \in \mathcal{N}_2^w(v) \setminus \mathcal{N}_2^s(v). \quad (9)$$

This captures nodes that are connected at distance two in the undirected sense, but not reachable via directed paths. To account for reverse flow patterns—such as when node E in Figure 3 is the focal node—we repeat this selection on the reversed network. This ensures that corresponding nodes like E' are correctly placed at level 0 when node E would be considered.

We take the sizes to be $|\mathcal{N}_1(v)| = n$, $|\mathcal{N}_2^s(v)| = m$, and $|\mathcal{N}_2^w(v) \setminus \mathcal{N}_2^s(v)| = l - 1$, resulting in l nodes at level 0, n nodes at level 1, and m nodes at level 2. The resulting adjacency matrix for the network on the right in Figure 3 is then

$$\begin{array}{c} A \\ A' \\ B \\ C \\ D \\ E \\ E' \end{array} \left(\begin{array}{cc|ccc|cc} 0 & 0 & 1 & 1 & 1 & 0 & 0 \\ 0 & 0 & 1 & 1 & 1 & 0 & 0 \\ \hline 0 & 0 & 0 & 0 & 0 & 1 & 1 \\ 0 & 0 & 0 & 0 & 0 & 1 & 1 \\ 0 & 0 & 0 & 0 & 0 & 1 & 1 \\ \hline 0 & 0 & 0 & 0 & 0 & 0 & 0 \\ 0 & 0 & 0 & 0 & 0 & 0 & 0 \end{array} \right). \quad (10)$$

As in the undirected case, structural constraints of the adjacency matrix are considered when calculating block-wise densities. For the upper-left block, score_{00} , the first row and column are excluded since all other level-0 nodes are second-order neighbours of the central node. Additionally, diagonal elements in all on-diagonal blocks (score_{00} , score_{11} and score_{22}) are excluded from density calculations, as self-loops are not present.

Adjustments are also made to score_{20} and score_{02} , which represent connections between the central node and second-order neighbours. The first row of block score_{20} and first column of block score_{02} are always zero and are therefore excluded.

No adjustments are applied to the remaining blocks, as the directionality among level-1 and level-2 nodes does not impose clear structural constraints.

The full adjacency matrix is thus partitioned into nine blocks, as shown in Equation (11), with block labels using zero-based indexing to reflect node levels 0, 1, and 2.

$$\begin{pmatrix} \mathbf{b}_{00} & \mathbf{b}_{01} & \mathbf{b}_{02} \\ \mathbf{b}_{10} & \mathbf{b}_{11} & \mathbf{b}_{12} \\ \mathbf{b}_{20} & \mathbf{b}_{21} & \mathbf{b}_{22} \end{pmatrix}, \quad (11)$$

where

$$\begin{aligned} \mathbf{b}_{00} &= (A_{i,j})_{1 \leq i, j \leq l} \\ \mathbf{b}_{01} &= (A_{i,j})_{1 \leq i \leq l, l+1 \leq j \leq l+n} \\ \mathbf{b}_{02} &= (A_{i,j})_{1 \leq i \leq l, l+n+1 \leq j \leq l+n+m} \\ \mathbf{b}_{10} &= (A_{i,j})_{l+1 \leq i \leq l+n, 1 \leq j \leq l} \\ \mathbf{b}_{11} &= (A_{i,j})_{l+1 \leq i, j \leq l+n} \\ \mathbf{b}_{12} &= (A_{i,j})_{l+1 \leq i \leq l+n, l+n+1 \leq j \leq l+n+m} \\ \mathbf{b}_{20} &= (A_{i,j})_{l+n+1 \leq i \leq l+n+m, 1 \leq j \leq l} \\ \mathbf{b}_{21} &= (A_{i,j})_{l+n+1 \leq i \leq l+n+m, l+1 \leq j \leq l+n} \\ \mathbf{b}_{22} &= (A_{i,j})_{l+n+1 \leq i, j \leq l+n+m} \end{aligned}$$

To compute the final score, we take the weighted average of the two blocks expected to have high density — according to the smurfing pattern in Equation (10) — and subtract the weighted average of the remaining blocks, which are expected to be sparse. As with the undirected case, a weighted average is used to account for block size, though a simple arithmetic mean is also a viable alternative. The use of the average ensures that the final GARG-AML score is between -1 and 1, to have consistent comparison and interpretation across datasets.

$$\begin{aligned} \text{score} &= \text{mean}(\text{score}_{01}, \text{score}_{12}) \\ &\quad - \text{mean}(\text{score}_{00}, \text{score}_{02}, \text{score}_{10}, \text{score}_{11}, \text{score}_{20}, \text{score}_{21}, \text{score}_{22}) \end{aligned} \quad (12)$$

The GARG-AML scores offer two key advantages. First, they approach 1 when a node's second-order neighbourhood resembles a smurfing pattern, providing a clear and interpretable signal for both automated detection and human investigation. This makes them easy to integrate into existing business rules or investigative workflows. Second, the method is highly scalable. Each score is computed independently using only a node's second-order neighbourhood, allowing for efficient parallel computation and low memory usage, even on large transaction networks.

Table 3: Overview of the parameters used to construct the synthetic data.

Parameter	Values	Barabási-Albert	Erdős-Rényi	Watts-Strogatz
Number of initial nodes	{100; 10,000; 100,000}	✓	✓	✓
Number of edges	{1; 2; 5}	✓	×	✓
Edge (rewiring) probability	{0.001; 0.01}	×	✓	✓
Number of smurfing patterns	{3; 5}	✓	✓	✓
Total number of combinations		18	12	36

4 Experimental Setup

4.1 Data

We experimentally evaluate the detection power of GARG-AML on multiple datasets. A first set concerns synthetic networks that we generate ourselves using various existing methods, to illustrate how GARG-AML scales with growing transaction networks and to evaluate how well it operates when faced with camouflaging tactics. In addition, the performance of GARG-AML is tested on two realistic open-source datasets. These mimic real-life transaction data; they include millions of observations of transactions, with only very few of these confirmed money laundering cases.

4.1.1 Synthetic Data

We generate synthetic networks of varying sizes using three generation methods, i.e., Barabási-Albert [4], Erdős-Rényi [15] and Watts-Strogatz [44]. The resulting networks have a range of different properties, e.g., scale-free, small world, etc., that allow the evaluation of GARG-AML across different network topologies.

Each of these methods has specific parameters that we vary to obtain a range of networks to test our method across different conditions. We summarize the ranges of these parameters in Table 3. The first parameter is the size of the network, which is subsequently set to 100, 10,000 and 100,000.

The other parameters have slightly different definitions depending on the method. The number of edges is set at 1, 2 or 5. For Barabási-Albert, this represents the number of nodes to which each new node connects, resulting in a large difference in degree across the nodes. For Watts-Strogatz, on the other hand, this is half the initial degree that all the nodes have before some of the edges are rewired.

The edge (rewiring) probability is set to 0.001 and 0.01. The Erdős-Rényi method uses this parameter to express the probability of having an edge between any two nodes. The Watts-Strogatz method starts with a fixed number of nodes, and uses this parameter to express the probability that an edge changes its end node (rewiring).

Smurfing patterns are injected after network generation. The three types of smurfing patterns that we consider in the experiments, and which are visualized in Figure 4, are the following:

1. **Separate:** The smurfing patterns are not connected to the rest of the network;
2. **External smurfs:** Mules are added between two existing entities in the network;
3. **Internal smurfs:** Existing nodes in the network are assigned the roles of sender, receiver and mule, and corresponding transactions are added.

In our experiments, each of the smurfing patterns is included either three or five times; see Table 3. The number of smurfs in each pattern is randomly chosen between two and ten. This is done to allow for smaller as well as larger smurfing patterns. A summary of all the synthetic datasets obtained is presented in Table 4.

Since we have information on which nodes are involved in which pattern for each dataset, we not only test the methods for money laundering detection in general; we also analyse how the methods perform on separate patterns. Similarly, we investigate how performance changes when money launderers apply higher levels of obfuscation methods.

4.1.2 Open-Source Data

As post-hoc injection of specific patterns may lead to detection bias [11] and altered topology [14], we also include data without this injection in the experiments to evaluate GARG-AML.

We use the HI-Small and LI-Large datasets, made publicly available by Altman et al. [3] and Egressy et al. [14], representing a relatively small dataset with high money laundering activity and a large dataset with low money laundering activity, respectively. Table 5 summarises the number of nodes, edges and the percentage of cases labelled as money laundering. Especially LI-Large closely resembles real-world transaction networks.

Table 4: Summary of the numbers of nodes and edges and money laundering percentages for the synthetic datasets according to the considered network generation parameters.

Dataset	n_nodes	m_edges	p_edges	n_patterns	Nodes	Edges	Labels
Barabási-Albert	100	1	-	3	145	199	46.9 %
Barabási-Albert	100	2	-	3	155	345	60.0 %
Barabási-Albert	100	5	-	3	141	582	50.35 %
Erdős-Rényi	100	-	0.001	3	151	122	52.32 %
Erdős-Rényi	100	-	0.01	3	153	155	60.78 %
Watts-Strogatz	100	1	0.001	3	144	204	48.61 %
Watts-Strogatz	100	1	0.01	3	146	216	52.05 %
Watts-Strogatz	100	2	0.001	3	131	268	40.46 %
Watts-Strogatz	100	2	0.01	3	146	316	52.74 %
Watts-Strogatz	100	5	0.001	3	151	618	52.32 %
Watts-Strogatz	100	5	0.01	3	145	616	53.1 %
Barabási-Albert	100	1	-	5	180	291	70.0 %
Barabási-Albert	100	2	-	5	179	385	69.83 %
Barabási-Albert	100	5	-	5	175	678	74.29 %
Erdős-Rényi	100	-	0.001	5	182	196	70.33 %
Erdős-Rényi	100	-	0.01	5	163	161	65.03 %
Watts-Strogatz	100	1	0.001	5	176	271	65.91 %
Watts-Strogatz	100	1	0.01	5	152	248	69.74 %
Watts-Strogatz	100	2	0.001	5	171	376	70.18 %
Watts-Strogatz	100	2	0.01	5	180	380	67.22 %
Watts-Strogatz	100	5	0.001	5	171	669	69.01 %
Watts-Strogatz	100	5	0.01	5	165	655	66.67 %
Barabási-Albert	10,000	1	-	3	10,037	10,101	0.69 %
Barabási-Albert	10,000	2	-	3	10,042	20,105	0.72 %
Barabási-Albert	10,000	5	-	3	10,043	50,103	0.77 %
Erdős-Rényi	10,000	-	0.001	3	10,044	5101	0.71 %
Erdős-Rényi	10,000	-	0.01	3	10,050	50,388	0.79 %
Watts-Strogatz	10,000	1	0.001	3	10,054	10,132	0.84 %
Watts-Strogatz	10,000	1	0.01	3	10,052	10,134	0.85 %
Watts-Strogatz	10,000	2	0.001	3	10,038	20,104	0.7 %
Watts-Strogatz	10,000	2	0.01	3	10,046	20,134	0.85 %
Watts-Strogatz	10,000	5	0.001	3	10,039	50,090	0.63 %
Watts-Strogatz	10,000	5	0.01	3	10,040	50,108	0.72 %
Barabási-Albert	10,000	1	-	5	10,059	10,171	1.15 %
Barabási-Albert	10,000	2	-	5	10,081	20,215	1.38 %
Barabási-Albert	10,000	5	-	5	10,072	50,167	1.2 %
Erdős-Rényi	10,000	-	0.001	5	10,079	5263	1.4 %
Erdős-Rényi	10,000	-	0.01	5	10,067	49,998	1.08 %
Watts-Strogatz	10,000	1	0.001	5	10,081	10,168	1.13 %
Watts-Strogatz	10,000	1	0.01	5	10,070	10,182	1.2 %
Watts-Strogatz	10,000	2	0.001	5	10,075	20,180	1.19 %
Watts-Strogatz	10,000	2	0.01	5	10,071	20,190	1.24 %
Watts-Strogatz	10,000	5	0.001	5	10,081	50,196	1.27 %
Watts-Strogatz	10,000	5	0.01	5	10,060	50,148	1.03 %
Barabási-Albert	100,000	1	-	3	100,044	100,099	0.07 %
Barabási-Albert	100,000	2	-	3	100,038	200,095	0.07 %
Barabási-Albert	100,000	5	-	3	100,043	500,093	0.07 %
Erdős-Rényi	100,000	-	0.001	3	100,033	498,969	0.06 %
Erdős-Rényi	100,000	-	0.01	3	100,044	4,998,019	0.07 %
Watts-Strogatz	100,000	1	0.001	3	100,050	100,124	0.08 %
Watts-Strogatz	100,000	1	0.01	3	100,045	100,096	0.07 %
Watts-Strogatz	100,000	2	0.001	3	100,044	200,114	0.07 %
Watts-Strogatz	100,000	2	0.01	3	100,041	200,116	0.08 %
Watts-Strogatz	100,000	5	0.001	3	100,042	500,114	0.07 %
Watts-Strogatz	100,000	5	0.01	3	100,045	500,116	0.08 %
Barabási-Albert	100,000	1	-	5	100,063	100,167	0.11 %
Barabási-Albert	100,000	2	-	5	100,069	200,175	0.12 %
Barabási-Albert	100,000	5	-	5	100,065	500,159	0.12 %
Erdős-Rényi	100,000	-	0.001	5	100,087	501,039	0.14 %
Erdős-Rényi	100,000	-	0.01	5	100,076	4,997,365	0.13 %
Watts-Strogatz	100,000	1	0.001	5	100,061	100,166	0.11 %
Watts-Strogatz	100,000	1	0.01	5	100,058	100,134	0.1 %
Watts-Strogatz	100,000	2	0.001	5	100,065	200,154	0.11 %
Watts-Strogatz	100,000	2	0.01	5	100,059	200,154	0.11 %
Watts-Strogatz	100,000	5	0.001	5	100,074	500,176	0.12 %
Watts-Strogatz	100,000	5	0.01	5	100,068	500,166	0.11 %

Table 5: The summary of the two IBM datasets, representing the number of nodes, edges and the percentage of instances labelled as money laundering (ML).

Dataset	# nodes	# edges	percentage ML
HI-Small	515 080	5 078 345	0.1%
LI-Large	2 054 390	176 066 557	0.05%

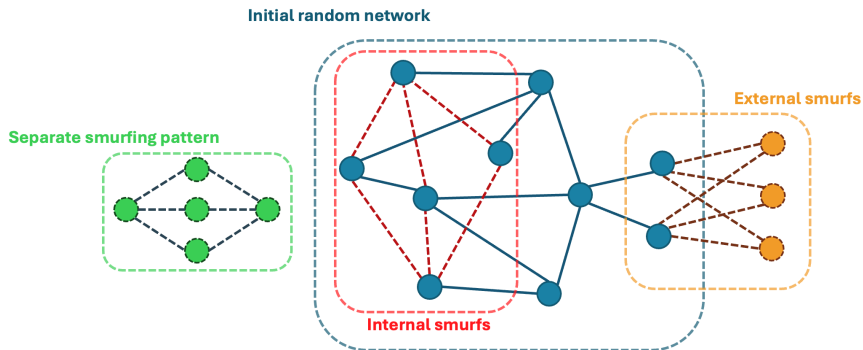


Figure 4: Illustration of a random network in which three different methods of injecting smurfing patterns are presented. The solid lines indicate nodes and edges of the original network, whereas the dotted lines indicate injected nodes and edges that correspond to smurfing.

Table 6: The distribution of the different types of money laundering transaction patterns for the two synthetic datasets.

Type of pattern	HI-Small	LI-Large
Fan-out	342	1 985
Fan-in	318	1 935
Gather-scatter	716	3 857
Scatter-Gather	626	3 694
Cycle	287	1 871
Random	191	1 458
Bipartite	263	1 807
Stack	466	2 854
Not classified	1 968	81 143
Total number of transactions	5 078 345	176 066 557

The two datasets are generated using the same simulator [3, 14], which models financial transactions in a virtual world involving individuals, companies, and banks. A subset of these transactions is labelled as money laundering. Since the full transaction graph is available, the authors were able to assign detailed labels, categorizing transaction streams into eight distinct types: fan-out, fan-in, gather-scatter, scatter-gather, simple cycle, random, bipartite, and stack.

Among these, the scatter-gather and gather-scatter patterns—illustrated in Figure 1—represent the primary smurfing behaviour that GARG-AML aims to detect. The distribution of labelled patterns is shown in Table 6. It is worth noting that some transactions are labelled as money laundering but do not match any of the eight defined structural patterns. These are grouped under the category “not classified”, indicating that they are suspicious but not attributable to a specific laundering archetype.

The original labels in these datasets are provided at the edge level, while GARG-AML produces features at the node level. To bridge this gap, we aggregate labels per client by computing the ratio of labelled laundering transactions to the total number of transactions associated with each node. This ratio is interpreted as a propensity score for money laundering.

To generate binary labels, we compare each node’s propensity score against a set of predefined thresholds: 10%, 20%, 30%, 50% and 90%. A node is labelled as involved in money laundering if the proportion of its laundering-labelled transactions exceeds the selected threshold. The resulting label distributions are presented in Table 7 and Table 8, corresponding to the HI-Small and LI-Large datasets, respectively.

In many cases, fewer than 0.1% of accounts are assigned a positive label, highlighting the extreme class imbalance and difficulty of the classification task. Additionally, accounts with more than 90% of laundering-labelled transactions are extremely rare, which reflects the realistic behaviour of laundering entities mixing illicit flows with legitimate transactions to obfuscate detection.

Table 7: Percentage of instances labelled as 1 in the HI-Small dataset, for the different patterns at different thresholds.

In percentage (%)	10	20	30	50	90
Is Laundering	0.445	0.175	0.103	0.020	0.013
Fan-out	0.029	0.012	0.009	0.002	0.002
Fan-in	0.022	0.006	0.005	0.002	0.001
Gather-scatter	0.055	0.018	0.014	0.002	0.001
Scatter-gather	0.036	0.022	0.010	0.003	0.000
Cycle	0.019	0.013	0.005	0.000	0.000
Random	0.014	0.007	0.002	0.000	0.000
Bipartite	0.030	0.007	0.004	0.001	0.001
Stack	0.044	0.021	0.011	0.001	0.001

Table 8: Percentage (%) of instances labelled as 1 in the LI-Large dataset, for the different patterns at different thresholds.

In percentage (%)	10	20	30	50	90
Is Laundering	0.2162	0.0414	0.0192	0.0017	0.0004
Fan-out	0.0051	0.0020	0.0007	0.0000	0.0000
Fan-in	0.0049	0.0025	0.0015	0.0003	0.0000
Gather-scatter	0.0081	0.0040	0.0029	0.0003	0.0000
Scatter-gather	0.0147	0.0047	0.0022	0.0001	0.0000
Cycle	0.0087	0.0016	0.0006	0.0000	0.0000
Random	0.0056	0.0007	0.0001	0.0000	0.0000
Bipartite	0.0042	0.0010	0.0004	0.0000	0.0000
Stack	0.0095	0.0012	0.0003	0.0000	0.0000

4.2 Model Specification

The full GARG-AML calculation pipeline consists of multiple stages, beginning with pre-processing steps that prepare the network data for analysis, followed by the computation of the GARG-AML scores. We also introduce a possible extension of the GARG-AML method that applies tree-based methods. We describe this use cases in detail below to illustrate the versatility of GARG-AML. An overview of the complete pipeline is shown in Figure 5.

Transaction networks often exhibit a scale-free structure [39], which are characterized by the presence of a few nodes (accounts) with disproportionately high numbers of incoming and outgoing transactions. As a result, second-order neighbourhoods can become very large and can encompass an unmanageable number of nodes for score computation.

Therefore, we first partition the network into communities using the Louvain method [5]. This method consistently shows state-of-the-art performance for community detection, and scales well to large graphs [23, 50]. Communities

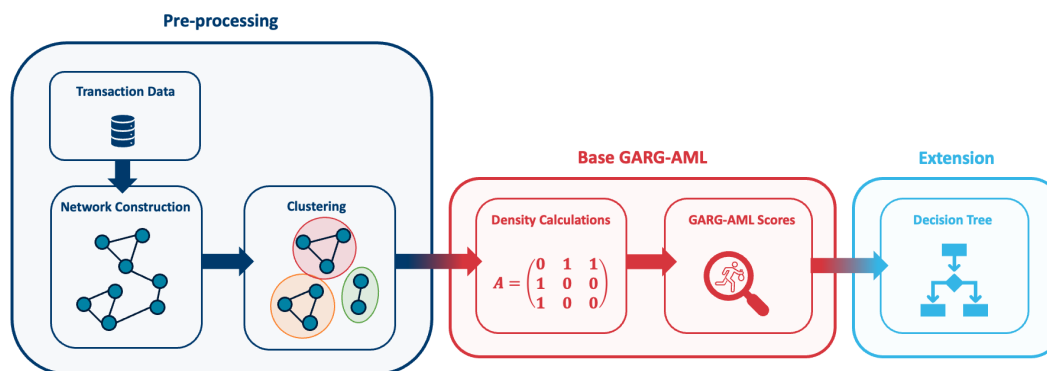


Figure 5: The pipeline of the GARG-AML method.

are identified on the basis of the undirected version of the transaction network, and only intra-community edges are retained—edges between communities are discarded.

However, the Louvain method can still produce overly large communities [17, 32]. To mitigate this, we use the implementation from NetworkX [21], which includes a resolution parameter inspired by the improvements proposed by Traag et al. [41]. In our experiments, we set this parameter to 10, which effectively encourages the algorithm to form smaller, more manageable communities, thus maintaining tractability in the GARG-AML score computation.

After pre-processing the network using the Louvain method, we calculate the block densities as described above via Equation (8) and Equation (12).

As a possible extension, we apply a decision tree and gradient boosting classifier with features on the basis of the GARG-AML scores. These include the original score as before, which is enhanced with summary statistics of each node’s first-order neighbours, i.e., the minimal, mean and maximal values of the GARG-AML scores as well as the standard deviation of the neighbours’ scores. Since successful smurfing involves many smurfs, we also include each node’s degree and the summary statistics—minimum, mean, maximum and standard deviation—of the degrees of the node’s neighbours.

The goal of including these extra features is to capture more complex neighbourhood structures that may not be evident from the scores alone. In particular, this helps reduce false positives—for example, a linear chain of three nodes may yield a perfect score, even though a single “smurf” is insufficient evidence of an actual laundering operation.

Applying this on the undirected and directed network results in four additional model. We use a 70-30 stratified train-test split for evaluation. This split is performed on the resulting feature table, not the network itself. For the decision tree, we use the Gini criterion and require that each leaf contain at least ten samples. The gradient boosting classifier consists of 100 trees with a maximal depth of three and a learning rate of 0.1. We require that each leaf node should contain at least 10 observations.

We benchmark GARG-AML and its extension against established state-of-the-art methods, namely, AutoAudit [24] and FlowScope [27]. For both methods, we use the implementations provided by the authors and retain their default settings.

Various small adaptations are necessary. AutoAudit returns an optimal reordering of indices in the adjacency matrix. However, this reordering affects only part of the matrix and may depend on the arbitrary labelling of nodes. To ensure robustness, we repeat the experiments three times with random initialization of the node indices and report the average results. Both methods also return an ordering of transactions resulting from the n different iterations. To reflect the decreasing level of certainty, the first group gets prediction 1, the second $\frac{n-1}{n}$ and so on until the final, n th, group gets score $\frac{1}{n}$. All other nodes that were not returned by the methods get score 0.

Algorithm 1 GARG-AML Score Calculation

Input: Network $G(V, E)$

Output: GARG-AML propensity score(s)

```

1: Calculate communities using Louvain method [5]
2: Remove inter-community edges
3: if Directed score then
4:   for node  $v \in V$  do
5:     Extract second order neighbourhood of  $v$ 
6:     Distribute neighbours over level 0, 1 and 2
7:     Define the adjacency matrix with level 0, 1 2.
8:     Define the nine blocks using Equation (11)
9:     Calculate score via Equation (12)
10:  end for
11: else
12:  for node  $v \in V$  do
13:    Extract second order neighbourhood of  $v$ 
14:    Define the adjacency matrix using  $v$ ,  $\mathcal{N}_2(v)$  and  $\mathcal{N}_1(v)$ 
15:    Define the three blocks using Equations (2)-(4)
16:    Calculate score via Equation (8)
17:  end for
18: end if
19: return: scores

```

4.3 Evaluation

Two key aspects are critical for business adoption. The first is **model performance**—a robust model must accurately detect money laundering while keeping false positives to a minimum. The second is **scalability**. Real-world transaction datasets are massive, with banks processing thousands to millions of transactions daily. Therefore, any proposed method must scale efficiently to such volumes. Accordingly, the evaluation of the methods focuses on these two dimensions.

For performance evaluation, the GARG-AML scores are assessed against ground-truth labels. The evaluation is conducted using the area under the receiver operating characteristic curve (AUC-ROC) and the area under the precision-recall curve (AUC-PR). These scores are also used to rank the methods, where the best-performing method receives rank 1, the second-best method receives rank 2, and so on.

While AUC-ROC is a widely used metric for binary classification, it may not be sufficient for anti-money laundering (AML) datasets, which are often highly imbalanced—typically with fewer than 0.1% observations flagged as laundering money. To address this imbalance, we include AUC-PR, which has been shown to be a more reliable performance metric under situations of extreme label imbalance [9, 33]. In general terms, the AUC-PR is the expected average precision when a random recall threshold is selected. In other words, the AUC-PR measures the model’s ability to identify positive examples correctly while minimising false positives across all possible threshold values. The AUC-PR specifically focuses on the model’s precision in identifying the positive class at various recall thresholds.

Scalability is assessed in terms of calculation time. In addition to runtime, memory usage is also a key factor. We also report any instances where methods fail due to memory limitations. All the experiments were conducted on the Flemish Supercomputer (VSC) with an Intel Xeon Platinum 8360Y CPU and 200 GB of memory. Each experiment was constrained to a time budget of 16 hours, the maximum on the VSC.

4.4 Statistical Test

The statistical significance of the difference in ranks is evaluated using the Friedman test [18, 19] and the post hoc Nemenyi test [31], as described by Demšar [10]. It compares the performance of the k different methods across the N datasets. If we take r_i^j to be the rank of method j on dataset i for some performance metric, then the average performance across all datasets is equal to $R_j = \frac{1}{N} \sum_i r_i^j$. In our experiments, the Friedman and Nemenyi statistical tests compare the ranks of the 8 (k) methods across the 66 (N) synthetic datasets. We apply a significance level of 0.05 for these tests.

The null hypothesis of the Friedman test is that the average ranks R_j are equal, and the Friedman statistic is equal to

$$Q = \frac{12N}{k(k+1)} \left[\sum_j R_j^2 - \frac{k(k+1)^2}{4} \right].$$

The Friedman statistic follows a χ_{k-1}^2 distribution under this null hypothesis.

Rejecting the null hypothesis indicates that significant differences are present among the methods. We then proceed with the post hoc Nemenyi test, which finds that the performances of two methods are significantly different at level α if their respective average ranks differ by at least the critical difference (CD):

$$CD = q_\alpha \sqrt{\frac{k(k+1)}{6N}},$$

where critical levels q_α are provided by Demšar [10]. We visualize the results using CD diagrams [10] for the AUC-ROC and AUC-PR.

5 Results and Discussion

The results are presented in two parts. First, we present and discuss the scalability of the methods. Afterward, we show the results for the performance and the CD diagrams.

5.1 Scalability

Figure 6 and Figure 7 shows the calculation times across the various network sizes of the synthetic data and IBM datasets, respectively. The time in Figure 6 is shown on a logarithmic scale since this provides a better distinction among the methods across dataset sizes. These results indicate that FlowScope is the fastest of all methods, although

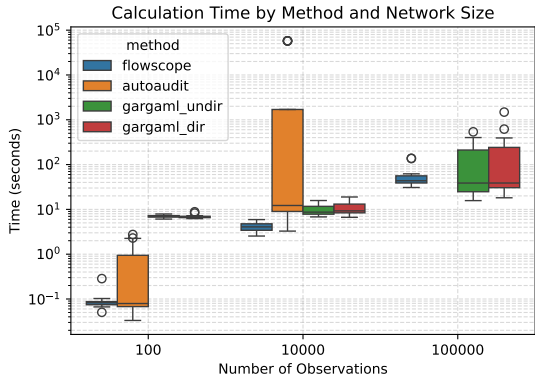


Figure 6: Box plot of the run time for each method on a logarithmic scale over the three different sizes of synthetic datasets. From left to right are FlowScope, AutoAudit, undirected GARG-AML and directed GARG-AML scores.

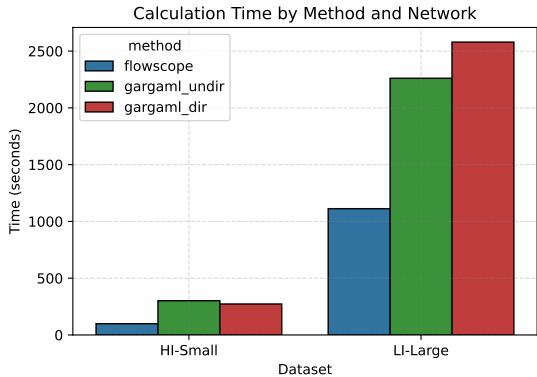


Figure 7: Bar plot of the run time for each method on a logarithmic scale over the two IBM datasets. From left to right are FlowScope, undirected GARG-AML and directed GARG-AML scores.

GARG-AML seems to scale better to larger datasets, as the calculation time increases much more slowly. In contrast, AutoAudit—although quite fast in the beginning—has difficulties with networks of the largest size. In addition, the distribution of the calculation time of AutoAudit is much wider and has more outliers, which indicates that it is highly sensitive to the network topology.

Another key observation is that AutoAudit consistently runs out of time—exceeding 16 hours—on Watts-Strogatz networks of size 10,000. This is reflected by setting the out-of-time results equal to 16 hours (57,600 seconds) in Figure 6, which results in outliers for AutoAudit. For the larger networks, i.e. the synthetic network of size 100,000 and the IBM datasets, AutoAudit exceeds the available memory. Hence, the results for AutoAudit are omitted entirely from Figure 7.

5.2 Performance

5.2.1 Synthetic Data

The results are presented according to the different injected patterns. These are provided in Figure 8, with their corresponding ranks presented in Figure 9.

The AUC-PR values are more spread out than the AUC-ROC values. This is caused by the varying level of class imbalance, as shown in Table 4. For a model with random label predictions, the AUC-ROC is always 0.5, regardless of the label distribution, whereas the AUC-PR equals the proportion of positive labels, which leads to the high variance shown in Figure 8.

Figure 8 indicates that, on average, the undirected GARG-AML scores consistently showing great performance. This performance is boosted when combining the GARG-AML scores with the tree-based learners. In comparison, the performance of AutoAudit is less stable. Here, we set all the AUC-ROC and AUC-PR values to 0 when the method runs out of time or out of memory to allow for a full comparison of the ranks. For these cases, AutoAudit ranks last compared with the other methods.

The ranks in Figure 9 corroborate the results from before. We can see more clearly that combining the tree-based learners with the scores and summary statistics of the node’s neighbours score better than the other methods, even when just applying a simple decision tree. We test the statistical significance of the difference in average rank using the Friedman test. For all the cases, the Friedman test rejects the null hypothesis, which indicates that significant differences between the ranks are present.

The post hoc Nemenyi test is used to discern which methods have significantly different average ranks. The results are shown in Figure 10 and Figure 11 for the AUC-ROC and AUC-PR, respectively. Here, again the tree-based methods differ significantly from most other methods, and the undirected scores on their own also obtain strong performance. For the existing mules patterns, however, it seems that the best performing models do not differ significantly from FlowScope.

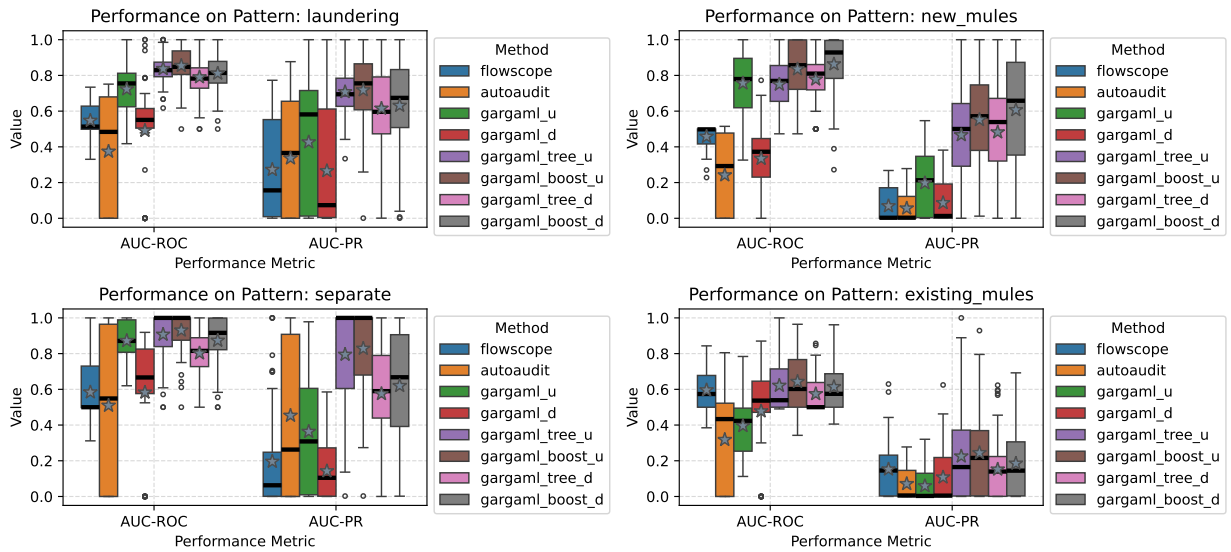


Figure 8: AUC-ROC and AUC-PR values of the compared methods across all synthetic datasets, with the split-on money laundering pattern.

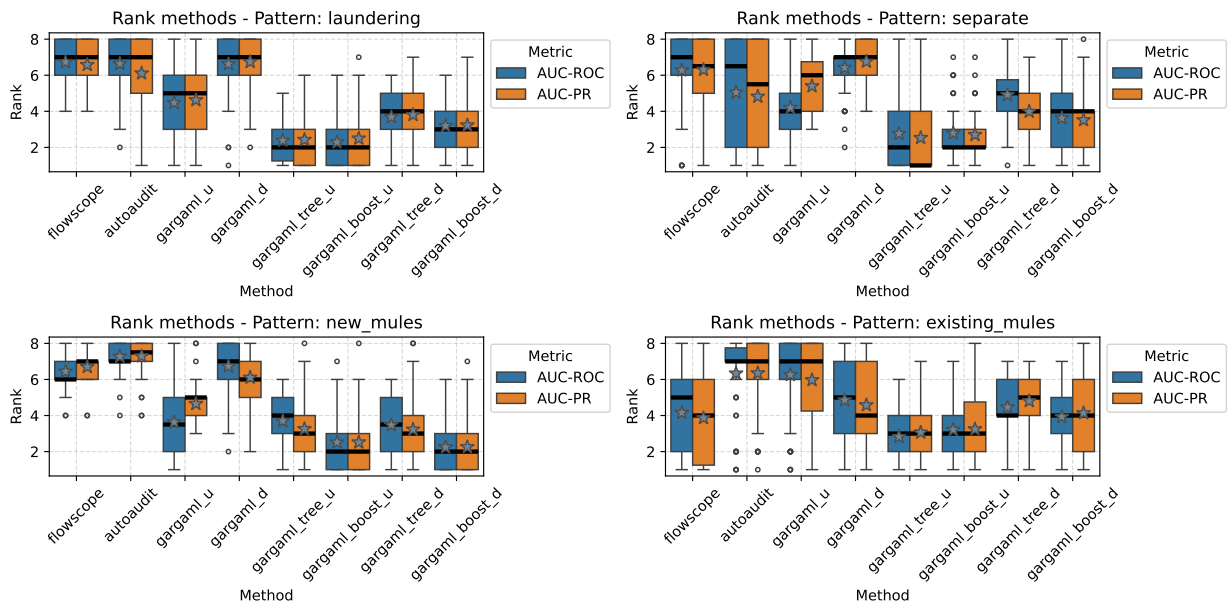


Figure 9: Ranks of the AUC-ROC and AUC-PR values of the compared methods across all synthetic datasets, with the split-on money laundering pattern, where rank 1 indicates the best performance and rank 8 indicates the worst performance.

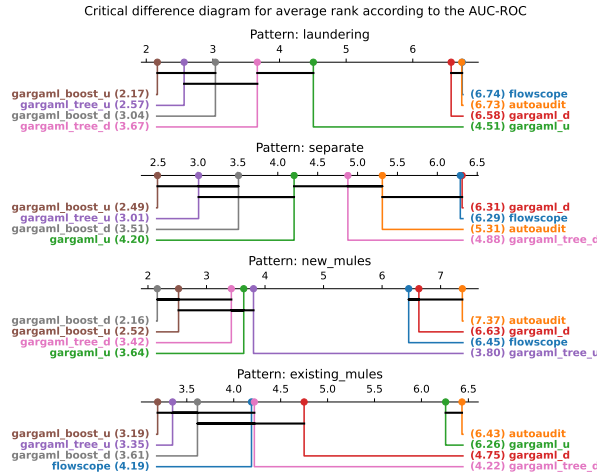


Figure 10: Critical distance plots of the average ranks according to the AUC-ROC for the considered patterns.

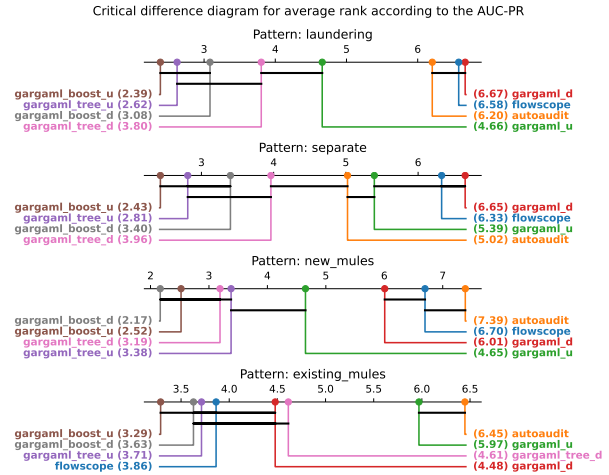


Figure 11: Critical distance plots of the average ranks according to the AUC-PR for the considered patterns.

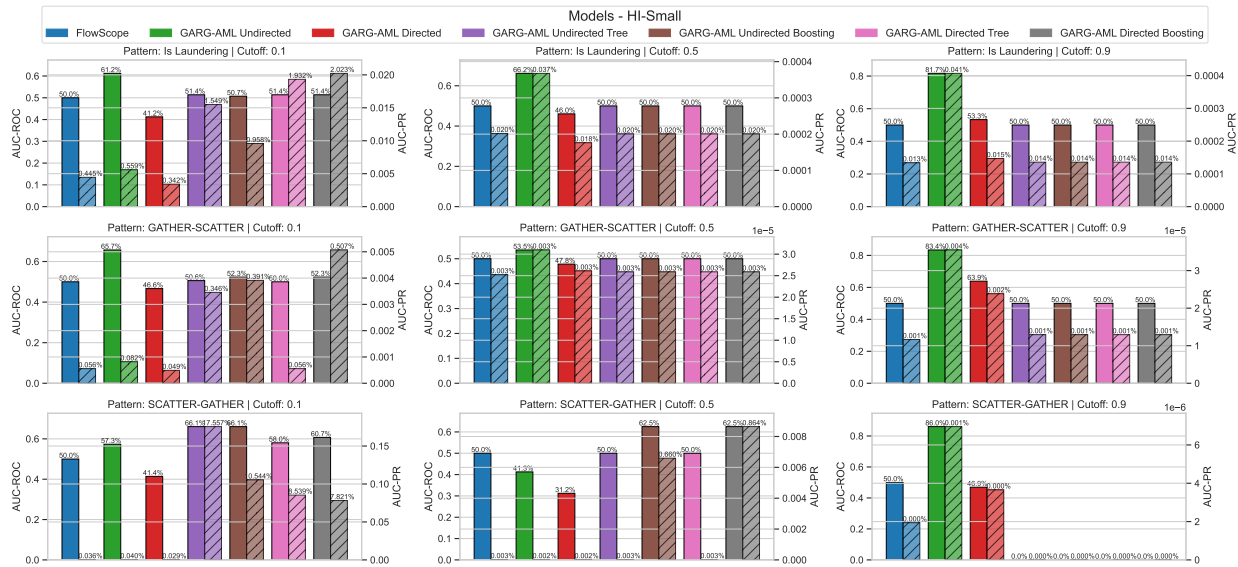


Figure 12: The AUC-ROC (solid bars) and AUC-PR (hatched bars) results on the HI-Small IBM dataset on the money laundering and smurfing labels across different thresholds.

5.2.2 IBM Data

This section presents the results on the IBM datasets for the smurfing patterns, i.e., gather-scatter and scatter-gather, and the full ‘Is Laundering’ label. The thresholds applied for binary label definition are 0.1, 0.2 and 0.9. The results for the HI-Small and LI-Large datasets are presented in Figure 12 and Figure 13, respectively. The results for all patterns and thresholds are provided in Appendix A.

Similar to the results on the synthetic data, the undirected version of the GARG-AML scores obtain best performance for almost all cases for the AUC-ROC values, followed by the tree-based models. For both datasets, the undirected GARG-AML scores give great results for the general laundering cases as well, which include more patterns than just smurfing.

For the lower threshold values, we see a significant improvement of AUC-PR across the tree-based methods. This results from these methods being able to better capture the interaction among a node’s GARG-AML score and those of its neighbours. This reduces the false positives compared to the basic score, resulting in a much higher AUC-PR. Therefore, on lower thresholds, we conclude that the tree-based methods are better suited for smurfing detection.

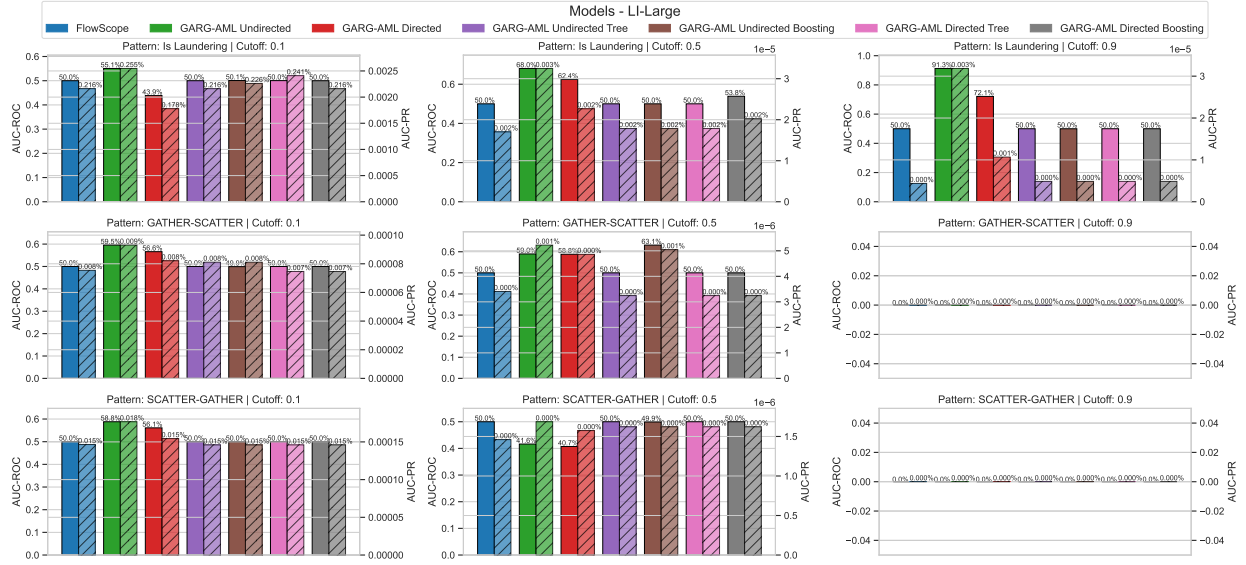


Figure 13: The AUC-ROC (solid bars) and AUC-PR (hatched bars) results on the LI-Large IBM dataset on the money laundering and smurfing labels across different thresholds. Some panels are empty, due to the absence of positive labels for these cases.

For the highest thresholds the basic GARG-AML scores provide great performance, with AUC-ROC above 80%. In these cases, only clients are labelled that have 90% or more of their transactions involved in money laundering. Therefore, low levels of obfuscation are present and the transaction patterns are very close to pure smurfing, making them easily recognisable by GARG-AML.

The tree-based models, on the other hand, seem to perform poorly, in line with FlowScope. It seems that the class imbalance (see also Table 7 and Table 8) is too extreme in these cases, resulting in the model’s inability to train properly.

6 Limitations

This work has limitations related to both data availability and methodology.

6.1 Limitations in the Data

GARG-AML assumes full visibility into all transactions, which is rarely the case in practice [3, 40, 13]. Banks typically have access only to transactions that involve their own clients, including sender and receiver account numbers and client attributes. Transactions between two external accounts remain hidden, which makes second-order neighbourhoods incomplete. This can obscure smurfing structures or lead to incorrect classification (see Figure 14). Moreover, banks cannot link multiple third-party accounts that are owned by the same individual, thus further weakening pattern recognition.

6.2 Limitations in the Methodology

GARG-AML uses unweighted graph structures, ignoring transaction volume and timing. While these are simplifications, the resulting smurfing score remains interpretable and useful in downstream AML systems. Timing issues can be addressed by restricting analysis to shorter time windows, applying sliding windows, or comparing scores across temporal blocks.

7 Conclusion

This paper introduces Graph-Aided Risk Grading for Anti-Money Laundering (GARG-AML), which is a novel approach for detecting smurfing by quantifying the structural similarity of nodes’ neighbourhoods to known money laundering patterns via density-based features in the adjacency matrix.

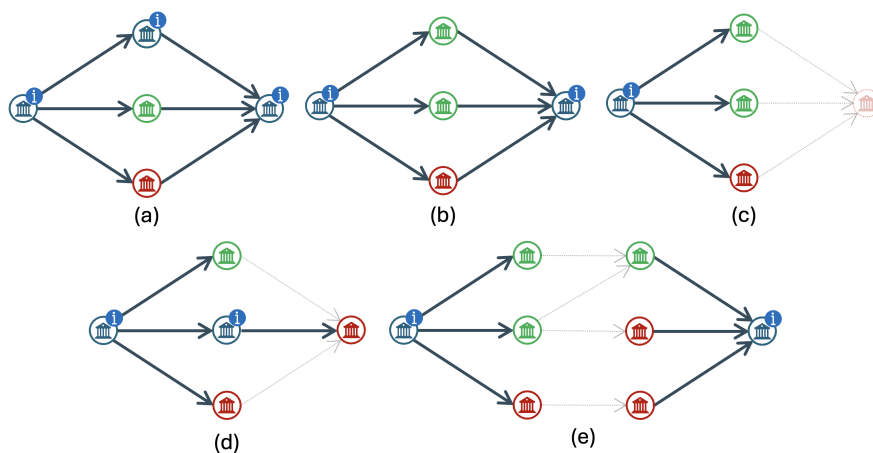


Figure 14: Illustration of smurfing over different banks, which are represented by different colours. The (i)-icon indicates that the main (blue) bank has all client information about the corresponding account. The dotted lines indicate that the bank is unaware of these transactions/accounts.

We validated GARG-AML on several synthetic datasets and compared it to state-of-the-art smurfing detection methods. The results of the experiments show that GARG-AML achieves strong detection power, with state-of-the-art performance of GARG-AML scores, and excellent scalability for large networks. Unlike approaches that are based on complex optimization techniques or machine learning models, GARG-AML relies on domain expertise and straightforward density-based calculations.

While GARG-AML is not a complete solution for smurfing detection, it offers two key advantages over existing methods: (1) it produces interpretable features—either as separate densities or a single composite score—that can be seamlessly integrated into AML systems, and (2) it is computationally efficient, with parallelisable and memory-light calculations, thus enabling practical deployment in real-world settings.

Future work will explore (i) treating individual densities as features in classification models and (ii) extending the methodology to incorporate transaction timing and volume, as well as generalising it to other anomalous transaction patterns.

Detecting smurfs is also an important research area for network security and intrusion detection [49, 38]. Further research could analyse whether similar featurisation of the patterns is possible for denial of service (DoS) or similar attacks.

Acknowledgments

This work was supported by the Research Foundation – Flanders (FWO) [grant number 1SHEN24N] and by the BNP Paribas Fortis Chair in Fraud Analytics. The resources and services used in this work were provided by the VSC (Flemish Supercomputer Center), funded by the Research Foundation - Flanders (FWO) and the Flemish Government.

Author Contributions

Bruno Deprez: Conceptualization, Data Curation, Methodology, Formal Analysis, Software, Visualization, Writing—Original Draft.

Bart Baesens: Conceptualization, Supervision, Writing—Review & Editing.

Tim Verdonck: Conceptualization, Supervision, Writing—Review & Editing.

Wouter Verbeke: Conceptualization, Project administration, Supervision, Writing—Review & Editing.

Declaration of Competing Interest

The authors declare that they have no known competing financial interests or personal relationships that could have appeared to influence the work reported in this paper.

References

- [1] 1999. URL <https://data.world/lpetrocelli/czech-financial-dataset-real-anonymized-transactions>.
- [2] Ismail Alarab, Simant Prakoonwit, and Mohamed Ikbal Nacer. Competence of graph convolutional networks for anti-money laundering in bitcoin blockchain. In *Proceedings of the 2020 5th International Conference on Machine Learning Technologies, ICMLT '20*, page 23–27, New York, NY, USA, 2020. Association for Computing Machinery. ISBN 9781450377645. doi:[10.1145/3409073.3409080](https://doi.org/10.1145/3409073.3409080). URL <https://doi.org/10.1145/3409073.3409080>.
- [3] Erik Altman, Jovan Blanuša, Luc von Niederhäusern, Beni Egressy, Andreea Anghel, and Kubilay Atasu. Realistic synthetic financial transactions for anti-money laundering models. In A. Oh, T. Naumann, A. Globerson, K. Saenko, M. Hardt, and S. Levine, editors, *Advances in Neural Information Processing Systems*, volume 36, pages 29851–29874. Curran Associates, Inc., 2023. URL https://proceedings.neurips.cc/paper_files/paper/2023/file/5f38404edff6f3f642d6fa5892479c42-Paper-Datasets_and_Benchmarks.pdf.
- [4] Albert-László Barabási and Réka Albert. Emergence of scaling in random networks. *Science*, 286(5439):509–512, 1999. ISSN 0036-8075.
- [5] Vincent D Blondel, Jean-Loup Guillaume, Renaud Lambiotte, and Etienne Lefebvre. Fast unfolding of communities in large networks. *Journal of Statistical Mechanics: Theory and Experiment*, 2008(10):P10008, oct 2008. doi:[10.1088/1742-5468/2008/10/P10008](https://doi.org/10.1088/1742-5468/2008/10/P10008). URL <https://dx.doi.org/10.1088/1742-5468/2008/10/P10008>.
- [6] Richard J. Bolton and David J. Hand. Statistical Fraud Detection: A Review. *Statistical Science*, 17(3):235 – 255, 2002. doi:[10.1214/ss/1042727940](https://doi.org/10.1214/ss/1042727940).
- [7] Mário Cardoso, Pedro Saleiro, and Pedro Bizarro. Laundrograph: Self-supervised graph representation learning for anti-money laundering. In *Proceedings of the Third ACM International Conference on AI in Finance, ICAIF '22*, page 130–138, New York, NY, USA, 2022. Association for Computing Machinery. ISBN 9781450393768. doi:[10.1145/3533271.3561727](https://doi.org/10.1145/3533271.3561727). URL <https://doi.org/10.1145/3533271.3561727>.
- [8] Zhiyuan Chen, Le Dinh Van Khoa, Ee Na Teoh, Amril Nazir, Ettikan Kandasamy Karuppiyah, and Kim Sim Lam. Machine learning techniques for anti-money laundering (aml) solutions in suspicious transaction detection: a review. *Knowledge and Information Systems*, 57(2):245–285, 2018. doi:[10.1007/s10115-017-1144-z](https://doi.org/10.1007/s10115-017-1144-z). URL <https://doi.org/10.1007/s10115-017-1144-z>.
- [9] Jesse Davis and Mark Goadrich. The relationship between precision-recall and roc curves. In *Proceedings of the 23rd International Conference on Machine Learning, ICML '06*, page 233–240, New York, NY, USA, 2006. Association for Computing Machinery. ISBN 1595933832. doi:[10.1145/1143844.1143874](https://doi.org/10.1145/1143844.1143874). URL <https://doi.org/10.1145/1143844.1143874>.
- [10] Janez Demšar. Statistical comparisons of classifiers over multiple data sets. *Journal of Machine Learning Research*, 7(1):1–30, 2006. URL <http://jmlr.org/papers/v7/demsar06a.html>.
- [11] Bruno Deprez, Toon Vanderschueren, Bart Baesens, Tim Verdonck, and Wouter Verbeke. Network analytics for anti-money laundering – a systematic literature review and experimental evaluation. *arXiv preprint arXiv:2405.19383*, 2024. URL <https://arxiv.org/abs/2405.19383>.
- [12] Rafał Dreżewski, Jan Sepielak, and Wojciech Filipkowski. The application of social network analysis algorithms in a system supporting money laundering detection. *Information Sciences*, 295:18–32, 2015. ISSN 0020-0255. doi:<https://doi.org/10.1016/j.ins.2014.10.015>. URL <https://www.sciencedirect.com/science/article/pii/S0020025514009979>.
- [13] Bogdan Dumitrescu, Andra Băltoiu, and Ștefania Budulan. Anomaly detection in graphs of bank transactions for anti money laundering applications. *IEEE Access*, 10:47699–47714, 2022. doi:[10.1109/ACCESS.2022.3170467](https://doi.org/10.1109/ACCESS.2022.3170467).
- [14] Béni Egressy, Luc von Niederhäusern, Jovan Blanuša, Erik Altman, Roger Wattenhofer, and Kubilay Atasu. Provably powerful graph neural networks for directed multigraphs. *Proceedings of the AAAI Conference on Artificial Intelligence*, 38(10):11838–11846, Mar. 2024. doi:[10.1609/aaai.v38i10.29069](https://doi.org/10.1609/aaai.v38i10.29069). URL <https://ojs.aaai.org/index.php/AAAI/article/view/29069>.
- [15] Paul Erdős and Alfréd Rényi. On random graphs. *Publicationes Mathematicae Debrecen*, 6(290-297):18, 1959.
- [16] FATF. *International Standards on Combating Money Laundering and the Financing of Terrorism & Proliferation*. FATF, Paris, France, 2012-2023. URL www.fatf-gafi.org/en/publications/Fatfrecommendations/Fatf-recommendations.html.
- [17] Santo Fortunato and Marc Barthélemy. Resolution limit in community detection. *Proceedings of the National Academy of Sciences*, 104(1):36–41, 2007. doi:[10.1073/pnas.0605965104](https://doi.org/10.1073/pnas.0605965104). URL <https://www.pnas.org/doi/abs/10.1073/pnas.0605965104>.

- [18] Milton Friedman. The use of ranks to avoid the assumption of normality implicit in the analysis of variance. *Journal of the American Statistical Association*, 32(200):675–701, 1937. doi:[10.1080/01621459.1937.10503522](https://doi.org/10.1080/01621459.1937.10503522). URL <https://www.tandfonline.com/doi/abs/10.1080/01621459.1937.10503522>.
- [19] Milton Friedman. A comparison of alternative tests of significance for the problem of m rankings. *The Annals of Mathematical Statistics*, 11(1):86–92, 1940. ISSN 00034851. URL <http://www.jstor.org/stable/2235971>.
- [20] Andrea Fronzetti Colladon and Elisa Remondi. Using social network analysis to prevent money laundering. *Expert Systems with Applications*, 67:49–58, 2017. ISSN 0957-4174. doi:<https://doi.org/10.1016/j.eswa.2016.09.029>. URL <https://www.sciencedirect.com/science/article/pii/S0957417416305139>.
- [21] Aric Hagberg, Daniel A. Schult, and Pieter J. Swart. Exploring network structure, dynamics, and function using networkx. In *Proceedings of the 7th Python in Science Conference (SciPy2008)*, page 11–15, 2008. URL <https://www.osti.gov/biblio/960616>.
- [22] Dattatray Vishnu Kute, Biswajeet Pradhan, Nagesh Shukla, and Abdullah Alamri. Deep learning and explainable artificial intelligence techniques applied for detecting money laundering—a critical review. *IEEE Access*, 9: 82300–82317, 2021.
- [23] Andrea Lancichinetti and Santo Fortunato. Community detection algorithms: A comparative analysis. *Phys. Rev. E*, 80:056117, 2009. doi:[10.1103/PhysRevE.80.056117](https://doi.org/10.1103/PhysRevE.80.056117).
- [24] Meng-Chieh Lee, Yue Zhao, Aluna Wang, Pierre Jinghong Liang, Leman Akoglu, Vincent S Tseng, and Christos Faloutsos. Autoaudit: Mining accounting and time-evolving graphs. In *2020 IEEE International Conference on Big Data (Big Data)*, pages 950–956. IEEE, 2020. doi:[10.1109/BigData50022.2020.9378346](https://doi.org/10.1109/BigData50022.2020.9378346).
- [25] Kevin J. Leonard. The development of a rule based expert system model for fraud alert in consumer credit. *European Journal of Operational Research*, 80(2):350–356, 1995. ISSN 0377-2217. doi:[https://doi.org/10.1016/0377-2217\(93\)E0249-W](https://doi.org/10.1016/0377-2217(93)E0249-W). URL <https://www.sciencedirect.com/science/article/pii/0377221793E0249W>.
- [26] Michael Levi and Peter Reuter. Money laundering. *Crime and justice*, 34(1):289–375, 2006. doi:[10.1086/501508](https://doi.org/10.1086/501508).
- [27] Xiangfeng Li, Shenghua Liu, Zifeng Li, Xiaotian Han, Chuan Shi, Bryan Hooi, He Huang, and Xueqi Cheng. Flowscope: Spotting money laundering based on graphs. *Proceedings of the AAAI Conference on Artificial Intelligence*, 34(04):4731–4738, 2020. doi:[10.1609/aaai.v34i04.5906](https://doi.org/10.1609/aaai.v34i04.5906). URL <https://ojs.aaai.org/index.php/AAAI/article/view/5906>.
- [28] Xiao Fan Liu, Xin-Jian Jiang, Si-Hao Liu, and Chi Kong Tse. Knowledge discovery in cryptocurrency transactions: A survey. *Ieee access*, 9:37229–37254, 2021. doi:[10.1109/ACCESS.2021.3062652](https://doi.org/10.1109/ACCESS.2021.3062652).
- [29] Wai Weng Lo, Gayan K. Kulatilleke, Mohanad Sarhan, Siamak Layeghy, and Marius Portmann. Inspection-l: self-supervised gnn node embeddings for money laundering detection in bitcoin. *Applied Intelligence*, 53(16):19406–19417, 2023. doi:[10.1007/s10489-023-04504-9](https://doi.org/10.1007/s10489-023-04504-9). URL <https://doi.org/10.1007/s10489-023-04504-9>.
- [30] John Madinger. *Money laundering: a guide for criminal investigators*. CRC Press, Boca Raton, 3rd ed. edition, 2012. ISBN 978-1-4398-6912-3.
- [31] Peter Bjorn Nemenyi. *Distribution-free multiple comparisons*. Princeton University, 1963.
- [32] Mark EJ Newman and Michelle Girvan. Finding and evaluating community structure in networks. *Physical review E*, 69(2):026113, 2004. URL <https://doi.org/10.1103/PhysRevE.69.026113>.
- [33] Brice Ozenne, Fabien Subtil, and Delphine Maucort-Boulch. The precision–recall curve overcame the optimism of the receiver operating characteristic curve in rare diseases. *Journal of clinical epidemiology*, 68(8):855–859, 2015.
- [34] Berkan Oztas, Deniz Cetinkaya, Festus Adedoyin, Marcin Budka, Gokhan Aksu, and Huseyin Dogan. Transaction monitoring in anti-money laundering: A qualitative analysis and points of view from industry. *Future Generation Computer Systems*, 159:161–171, 2024.
- [35] Mario Alfonso Prado-Romero, Christian Doerr, and Andrés Gago-Alonso. Discovering bitcoin mixing using anomaly detection. In Marcelo Mendoza and Sergio Velastín, editors, *Progress in Pattern Recognition, Image Analysis, Computer Vision, and Applications*, pages 534–541, Cham, 2018. Springer International Publishing. ISBN 978-3-319-75193-1.
- [36] Daniel Sánchez, MA Vila, L Cerda, and José-Maria Serrano. Association rules applied to credit card fraud detection. *Expert Systems with Applications*, 36(2, Part 2):3630–3640, 2009. doi:<https://doi.org/10.1016/j.eswa.2008.02.001>.
- [37] Ted E Senator, Henry G Goldberg, Jerry Wooton, Matthew A Cottini, AF Umar Khan, Christina D Klinger, Winston M Llamas, Michael P Marrone, and Raphael WH Wong. Financial crimes enforcement network ai system

- (fais) identifying potential money laundering from reports of large cash transactions. *AI magazine*, 16(4):21–21, 1995. doi:[10.1609/aimag.v16i4.1169](https://doi.org/10.1609/aimag.v16i4.1169).
- [38] Shiva Shadrooh and Kjetil Nørnvåg. Smotef: Smurf money laundering detection using temporal order and flow analysis. *Applied Intelligence*, 2024. doi:[10.1007/s10489-024-05545-4](https://doi.org/10.1007/s10489-024-05545-4). URL <https://doi.org/10.1007/s10489-024-05545-4>.
- [39] Michele Starnini, Charalampos E. Tsourakakis, Maryam Zamanipour, André Panisson, Walter Allasia, Marco Fornasiero, Laura Li Puma, Valeria Ricci, Silvia Ronchiadin, Angela Ugrinoska, Marco Varetto, and Dario Moncalvo. Smurf-based anti-money laundering in time-evolving transaction networks. In Yuxiao Dong, Nicolas Kourtellis, Barbara Hammer, and Jose A. Lozano, editors, *Machine Learning and Knowledge Discovery in Databases. Applied Data Science Track*, pages 171–186, Cham, 2021. Springer International Publishing. ISBN 978-3-030-86514-6. URL https://doi.org/10.1007/978-3-030-86514-6_11.
- [40] Haseeb Tariq and Marwan Hassani. Topology-agnostic detection of temporal money laundering flows in billion-scale transactions, 2023.
- [41] V. A. Traag, L. Waltman, and N. J. van Eck. From louvain to leiden: guaranteeing well-connected communities. *Scientific Reports*, 9(1):5233, 2019. doi:[10.1038/s41598-019-41695-z](https://doi.org/10.1038/s41598-019-41695-z). URL <https://doi.org/10.1038/s41598-019-41695-z>.
- [42] United Nations Office on Drugs and Crime. Money laundering. <https://www.unodc.org/unodc/en/money-laundering/overview.html>, (n.d.).
- [43] Rafaël Van Belle, Bart Baesens, and Jochen De Weerd. Catchm: A novel network-based credit card fraud detection method using node representation learning. *Decision Support Systems*, 164:113866, 2023. ISSN 0167-9236. doi:<https://doi.org/10.1016/j.dss.2022.113866>.
- [44] Duncan J. Watts and Steven H. Strogatz. Collective dynamics of ‘small-world’ networks. *Nature*, 393(6684):440–442, 1998. doi:[10.1038/30918](https://doi.org/10.1038/30918). URL <https://doi.org/10.1038/30918>.
- [45] Mark Weber, Giacomo Domeniconi, Jie Chen, Daniel Karl I. Weidele, Claudio Bellei, Tom Robinson, and Charles E. Leiserson. Anti-money laundering in bitcoin: Experimenting with graph convolutional networks for financial forensics, 2019.
- [46] Sarah N Welling. Smurfs, money laundering, and the federal criminal law: the crime of structuring transactions. *Fla. L. Rev.*, 41:287, 1989.
- [47] Jiajing Wu, Jieli Liu, Weili Chen, Huawei Huang, Zibin Zheng, and Yan Zhang. Detecting mixing services via mining bitcoin transaction network with hybrid motifs. *IEEE Transactions on Systems, Man, and Cybernetics: Systems*, 52(4):2237–2249, 2021. doi:[10.1109/TSMC.2021.3049278](https://doi.org/10.1109/TSMC.2021.3049278).
- [48] Lei Wu, Yufeng Hu, Yajin Zhou, Haoyu Wang, Xiapu Luo, Zhi Wang, Fan Zhang, and Kui Ren. Towards understanding and demystifying bitcoin mixing services. In *Proceedings of the Web Conference 2021, WWW ’21*, page 33–44, New York, NY, USA, 2021. Association for Computing Machinery. ISBN 9781450383127. doi:[10.1145/3442381.3449880](https://doi.org/10.1145/3442381.3449880). URL <https://doi.org/10.1145/3442381.3449880>.
- [49] Jin Yang, XiaoJie Liu, Tao Li, Gang Liang, and SunJun Liu. Distributed agents model for intrusion detection based on ais. *Knowledge-Based Systems*, 22(2):115–119, 2009. ISSN 0950-7051. doi:<https://doi.org/10.1016/j.knosys.2008.07.005>. URL <https://www.sciencedirect.com/science/article/pii/S0950705108001391>.
- [50] Zhao Yang, René Algesheimer, and Claudio J. Tessone. A comparative analysis of community detection algorithms on artificial networks. *Scientific Reports*, 6(1):30750, 2016. doi:[10.1038/srep30750](https://doi.org/10.1038/srep30750). URL <https://doi.org/10.1038/srep30750>.
- [51] Maria Zhdanova, Jürgen Repp, Roland Rieke, Chrystel Gaber, and Baptiste Hemery. No smurfs: Revealing fraud chains in mobile money transfers. In *2014 Ninth International Conference on Availability, Reliability and Security*, pages 11–20. IEEE, 2014. doi:[10.1109/ARES.2014.10](https://doi.org/10.1109/ARES.2014.10).
- [52] Pengfei Zhu and Qinghua Hu. Rule extraction from support vector machines based on consistent region covering reduction. *Knowledge-Based Systems*, 42:1–8, 2013. ISSN 0950-7051. doi:<https://doi.org/10.1016/j.knosys.2012.12.003>. URL <https://www.sciencedirect.com/science/article/pii/S095070511200336X>.



Figure A.1: The AUC-ROC (solid bars) and AUC-PR (hatched bars) results on the HI-Small IBM dataset across all thresholds and patterns.

A Full Results IBM Data

In this part of the appendix, we provide the full results on the IBM datasets. These include all different patterns defined by Altman et al. [3]. The binary labels are defined using the threshold values 0.1, 0.2, 0.3, 0.5 and 0.9. The results on the HI-Small and LI-Large datasets are provided in Figure A.1 and Figure A.2, respectively.



Figure A.2: The AUC-ROC (solid bars) and AUC-PR (hatched bars) results on the LI-Large IBM dataset across all thresholds and patterns.